

Date of publication xxxx 00, 0000, date of current version xxxx 00, 0000.

Digital Object Identifier 10.1109/ACCESS.2017.Doi Number

Surface Defect Classification for Hot-Rolled Steel Strips by Selectively Dominant Local Binary Patterns

Qiwu Luo^{1,2}, Member, IEEE, Xiaoxin Fang², Yichuang Sun³, Senior Member, IEEE, Li Liu^{4,5}, Jiaqiu Ai⁶, Member, IEEE, Chunhua Yang¹, Member, IEEE, and Oluyomi Simpson³, Member, IEEE

¹ School of Automation, Central South University, Changsha 410083, China.

² School of Electrical and Automation Engineering, Hefei University of Technology, Hefei 230009, China.

³ School of Engineering and Technology, University of Hertfordshire, Hatfield AL10 9AB, U.K.

⁴ Center for Machine Vision and Signal Analysis, University of Oulu, Oulu 90014, Finland.

⁵ College of System Engineering, National University of Defense Technology, Changsha 410073, China.

⁶ School of Computer Science and Information Engineering, Hefei University of Technology, Hefei 230009, China.

Corresponding author: Qiwu Luo (luoqiwu@hfut.edu.cn).

This work was supported in part by the National Natural Science Foundation of China under Grant 51704089 and Grant 61701157, in part by the Anhui Provincial Natural Science Foundation of China under Grant 1808085QF190 and Grant 1808085QF206, in part by the China Postdoctoral Science Foundation under Grant 2017M621996, in part by the Fundamental Research Funds for the Central Universities of China under Grant JZ2018YYPY0296.

ABSTRACT Developments in defect descriptors and computer vision-based algorithms for automatic optical inspection (AOI) allows for further development in image-based measurements. Defect classification is a vital part of an optical-imaging-based surface quality measuring instrument. The high-speed production rhythm of hot continuous rolling requires ultra-rapid response to every component as well as algorithms in AOI instrument. In this paper, a simple, fast, yet robust texture descriptor, namely selectively dominant local binary patterns (SDLBP), is proposed for defect classification. Firstly, an intelligent searching algorithm with a quantitative thresholding mechanism is built to excavate the dominant non-uniform patterns (DNUPs). Secondly, two convertible schemes of pattern code mapping are developed for binary encoding of all uniform patterns and DNUPs. Thirdly, feature extraction is carried out under SDLBP framework. Finally, an adaptive region weighting (ARW) method is built for further strengthening the original nearest neighbor classifier (NNC) in the feature matching stage. Extensive experiments carried out on an open texture database (Outex) and an actual surface defect database (Dragon) indicate that our proposed SDLBP yields promising performance on both classification accuracy and time efficiency.

INDEX TERMS Automatic optical inspection (AOI), image classification, local binary patterns (LBP), steel industry, surface texture.

I. INTRODUCTION

Online defect inspection and quality inspection of broad surface are widely recognized important aspects for industrial manufacturing, especially for sheet materials. As a dominant product among flat steel, the hot-rolled steel strips occupy more than a half of all the products in iron and steel industry, which are not only the key raw materials for cold rolling in downstream, but also act as the fundamental materials for the related planar industries including aerospace, machinery, automobile, *etc.*

In recent years, an increasing number of steel mills have imported automatic optical inspection (AOI) instruments for

surface quality inspection of steel products, so as to enhance their commercial competitiveness. However, most AOI instruments are commercially occupied and their technique details are rarely reported for considering the intellectual property rights. The emergence of recent literature from scholars [1-7] which included new achievements and technology found a common AOI instrument supports two main functions: defect detection and defect classification. The former is to detect defects on the target material surface, the latter is to classify the types of detected defects in the former step. In general, the former detection process distinguishes defective regions from normal image of the

vast surface without identifying what kinds of defects they are. Further in the latter step, all uploaded images with suspicious defects will be recognized and labeled with distinct defect indexes. From goal-oriented aspect, the first defect detection is the foundation of the “quality problem close loop”, earlier defect inspection and location allow more timely and less economic losses. The closely followed defect classification is used for finishing product grading, which supports the relevant product pricing and distribution. A prominent obstacle in true online quality inspection, is the difficulty in attaining defect detection and classification with high accuracy whilst remaining time efficient.

At present, with newly developed techniques in pattern recognition and computer vision, the defect detection using both supervised manner [3, 4] and unsupervised manner [5, 6] has made impressive progress. The most recent reports on AOI instruments for hot-rolled steel strips indicate that the true positive detection rate has achieved about 96% [5], and the acceptable upper limit of rolling speed has been pushed to 20 m/s [6]. However, the surface defect classification has much improvement space due to the following challenges.

- 1) Unsatisfactory imaging environments. Hot-rolling lines involve multiple sufferings of high temperature, dense mist, heavy cooling water drops [6], uneven illumination [8], and aperiodic vibration [3, 9]. These limitations on image quality require sufficiently robust defect descriptors for the task of image classification, in order to address the challenges of large intra-class variation and minor inter-class distance [7, 26].
- 2) Continuous and massive image streams. The online dual-surface quality measurement for the average hot-rolled steel mills requires the surface AOI instrument to continuously process 2.56 Gbps of image data [7] to locate and identify defects. This working condition requires efficient defect descriptors for image classification, in order to satisfy the online quality measurement and effective production increase.

Hence, it is difficult to classify these defects either by complex learning models or by small-sample analysis through a simple thresholding. Recent literatures handled image classification tasks by using some feature extractors, for example, multi-scale geometric analysis (MGA) [10], 2-D wavelet technique [11], *etc.*, with classical classifiers such as support vector machine (SVM) [12], neural network [13], *etc.* In essential, some defect detection methods such as vector-valued regularized kernel function approximation [4] and Haar-Weibull-variance model [5] are mainly based on advanced classifiers. However, most of these methods emphasize more on classification accuracy than time efficiency. While the time efficiency is a very crucial indicator which decides whether these methods can be applied in real-world industrial practices.

As a result, the classification task is translated into exploring a series of accurate and efficient defect

descriptors for surface images. This paper investigated that the local binary patterns (LBP) method [14, 15] has merits of low computational complexity, meticulous descriptive quality, and illumination variation robustness [7, 16, 26]. Such descriptor and its variants, like completed LBP (CLBP) [17] and dominant LBP (DLBP) [18], have been widely applied on face recognition [19], moving object detection [20], texture description [21], texture feature extraction for quality measurement [22] or medical imagery [23], and fault diagnosis of mechanical component [24]. Some preliminary reports about LBP-based surface defect inspection can be available in current literatures [7, 25, 26].

This paper proposed a selectively dominant LBP (SDLBP) to quantitatively exploit the useful information from non-uniform patterns. As a result, employing SDLBP will serve as a means to overcome the aforementioned two challenges. The main contributions of this work are as follows:

- 1) A quantitative thresholding method is developed for SDLBP to avoid manual parameter regulation, which permits AOI instrument adapts to varied conditions in hot-rolling mills
- 2) Two convertible schemes of pattern code mapping are built to allow SDLBP can survive well among noisy images.
- 3) An adaptive region weighting scheme based on regional variances is set up to further improve classification accuracy.
- 4) The overall performances have been successfully verified on an open texture database (Outex) and an actual defect database (Dragon). It provides a referable case for AOI instruments of steel strip manufacturing.

The rest of this paper is organized as follows. Section II briefly reviews LBP and introduces study motivation. Section III explains technique details of the proposed SDLBP. Extensive experiments are demonstrated and discussed in Section IV. Finally, Section V concludes this research.

II. PRELIMINARIES AND MOTIVATION

A. Review of LBP

As shown in Fig. 1(a) and Fig. 1(b), given a test or training image sample $T[I \times J]$, an LBP [15] code is calculated by comparing the gray values of the center pixel g_c with its P symmetric neighbors g_p

$$LBP_{P,R}(x_c, y_c) = \sum_{p=0}^{P-1} 2^p s(g_p - g_c), s(t) = \begin{cases} 1, & t \geq 0 \\ 0, & t < 0 \end{cases} \quad (1)$$

Suppose the coordinate of g_c is $(0, 0)$, then the coordinates of g_p are $(R\cos(2\pi p/P), R\sin(2\pi p/P))$. The gray values of neighbors which are not fall in the image grids can be estimated by interpolation. Then the image $T[I \times J]$ can be represented by the following feature histogram made up of its LBP codes.

$$H(k) = \sum_{i=1}^I \sum_{j=1}^J f(LBP_{P,R}(i, j), k), f(x, y) = \begin{cases} 1, & x = y \\ 0, & \text{otherwise} \end{cases} \quad (2)$$

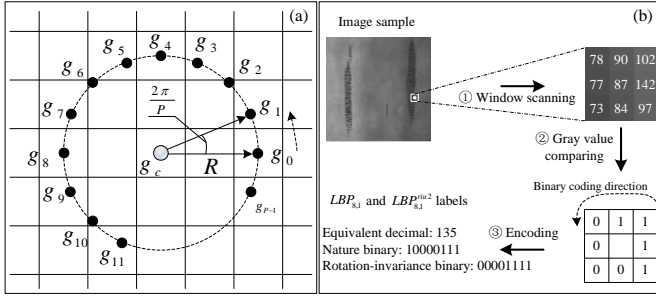


FIGURE 1. (a) Theoretical model of the $LBP_{P,R}$, and (b) an illustrative case, $LBP_{8,1}$.

where $k \in [0, K]$, and K is the maximal LBP pattern value. This original LBP operator (here after is denoted as $LBP_{P,R}^{orig}$) can achieve gray-scale invariance due to its robust suppression to the homomorphic gray change. An upgraded $LBP_{P,R}^{riu}$ operator was subsequently designed to achieve rotation invariance [15].

$$LBP_{P,R}^{riu} = \min \{ ROR(LBP_{P,R}, i) \mid i = 0, 1, \dots, P-1 \} \quad (3)$$

where $ROR(x, i)$ is a bitwise cyclic right shift operator. When just hold the rotationally-unique patterns can reduce the feature dimensionality effectively. Further, an evaluation criterion of pattern uniformity has been defined

$$\begin{cases} U(LBP_{P,R}) = U_{h2t}(LBP_{P,R}) + U_{intrm}(LBP_{P,R}) \\ U_{h2t}(LBP_{P,R}) = |s(g_{p-1} - g_c) - s(g_0 - g_c)| \\ U_{intrm}(LBP_{P,R}) = \sum_{p=1}^{P-1} |s(g_p - g_c) - s(g_{p-1} - g_c)| \end{cases} \quad (4)$$

where $U_{h2t}(\cdot)$ and $U_{intrm}(\cdot)$ respectively stand for the head-to-tail and intermediate spatial transitions between bit-wise '0' and '1' of the natural LBP codes. Then, $LBP_{P,R}^{riu2}$ operator was proposed for rotation invariant uniform patterns

$$LBP_{P,R}^{riu2} = \begin{cases} \sum_{p=1}^{P-1} s(g_p - g_c) & , U(LBP_{P,R}) \leq 2 \\ P+1 & , \text{otherwise} \end{cases} \quad (5)$$

where superscript $riu2$ represents the rotation invariant "uniform" patterns which have U values at most 2. Compared with $LBP_{P,R}^{orig}$, the output pattern labels produced by $LBP_{P,R}^{riu2}$ are dramatically decreased from 2^P to $P+2$. The mapping between these different pattern codes can be easily realized through a simple lookup table.

B. Analysis on Dominant Pattern Threshold (σ)

We found that useful descriptive information are implicitly included in non-uniform patterns. So patterns with higher occurrence frequency are selected as DNUPs for further improving image classification accuracy. Therefore, two issues need to be addressed for DNUPs pursuing. First, what distribution rules do the non-uniform patterns (NUPs) conform to? Second, how to set the threshold (σ) in DNUP pursuing process for best representation effect?

As for the first question, GCLBP [26] draws a preliminary practice recommendation that setting σ to 0.4-0.6 (always 0.5) could cover more than 90% of pattern

proportion. In this paper, we investigated that NUPs can be well modeled by Poisson distribution $P_1(x) = \lambda^x e^{-\lambda} / x!$, where $x = \mu\sigma$, $\sigma \in (0, 1)$, $P_1(\cdot)$ is growth rate of patterns, λ is the estimated incidence of random events per unit time (or unit area), and μ is an estimated factor, which can be set to 10. After some mathematical calculation, we can derive $P_1(x > 6)$ is almost equal to zero. Besides, feature matching on extra non-DNUPs are computationally expensive, hence, informative DNUPs selected by setting an appropriate σ are kept while extremely noisy non-DNUPs are discarded.

When it comes to the second problem, the relationship between σ to the figures of P_{ups} , P_{nups} , and τ can be expressed

$$\begin{cases} P_{ups} + P_{nups} \cdot \sigma \geq \tau \\ P_{ups} + P_{nups} = 1 \end{cases} \quad (6)$$

where P_{ups} is the proportion of uniform patterns (UPs) among all patterns, P_{nups} is the proportion of non-uniform patterns among all patterns, and τ is the targeted proportion of total selected patterns (UPs and DNUPs) among all patterns for image representation. After simple deduction, we can rewrite (6) as

$$\sigma \geq 1 - \frac{1 - \tau}{P_{nups}} \quad (7)$$

where P_{nups} can be easily obtained during the DNUPs training process. For an example, if given $P_{nups} = 15\%$, and $\tau = 90\%$, σ can be calculated as 33.33%.

C. Inspiration and Motivation

In our recent work [26], GCLBP provides a balanced scheme between advocates of pattern information (original LBP in [15]) and advocates of frequency information (DLBP in [18]) by excavating the implicit descriptive information from non-uniform patterns. However, besides the theoretical basis for selecting its threshold (σ) in DNUP pursuing process (addressed in Sec. II.B), there still remain some questions to be better answered about GCLBP. For example, how to flexibly generalize this kind of framework to other LBP variants? And is there any other auxiliary measure for further improving classification accuracy? For the first question, Lu et al. [27] realized recognition performance boost by borrowing the knowledge from related resolutions while preserving the underlying manifold structure of image. The key idea is to select reliable features while ignore unreliable features from in-depth understanding of image structure and resolution, which inspires us to study more descriptive pattern coding scheme to generalize GCLBP from imaging quality aspect (refer to Sec. III.B). When it comes to the second expectation, we investigated that a weighted deconvolution network was developed to balance the contributions presented in [28] for extracting useful information. Heuristically, we built an adaptive region weighting (ARW) scheme based on regional variances to enhance the traditional NNC for feature matching (refer to Sec. III.D).

This so-called ARW-NNC can further improve the classification accuracy of SDLBP-series descriptors.

III. SELECTIVELY DOMINANT LBP (SDLBP)

A. Dominant Non-uniform Features Pursuing

Statistically, dominant patterns with higher frequencies are more conducive to the representation of texture images [18]. In most cases, uniform patterns jointly play a dominant role while non-uniform patterns act as a supporting role [15], which is proportional to image line singularity and texture complexity. Algorithm 1, was developed to pursue the dominant non-uniform patterns (DNUPs) through selectively analyzing the pattern frequencies. First, the pattern label of each center pixel from each image is calculated according to (1). Second, the calculated pattern labels are discriminatively kept in two distinct buffer pools according to the pattern uniformity defined in (4), the statistics of two complementary histograms are finished during the same loop. Finally, several patterns with higher frequency of occurrence are selected as DNUPs, and the corresponding pattern labels are stored for the upcoming feature extraction. Given a targeted proportion of total selected patterns (τ), σ can be adaptively calculated according to (7).

B. Hybrid Pattern Code Mapping Mechanism

Originated from the fundamental pattern code mapping method $LBP_{P,R}^{riu2}$ [15], we build two targeted binary mapping schemes for SDLBP. The one is $SDLBP_{P,R}^{hriu2}$ (8), its superscript reflects the *hybrid rotation invariant uniform* patterns classified by judging the uniformity criterion $U()$ with number 2, the other is $SDLBP_{P,R}^{hriu2ln}$ (9), the extra 'ln' in its superscript stands for *lightweight nature* binaries of DNUPs.

$$SDLBP_{P,R}^{hriu2} = \begin{cases} \sum_{i=0}^{P-1} s(g_p - g_c), & U(LBP_{P,R}) \leq 2 \\ LBP_{P,R}^{riu2}, & U(LBP_{P,R}) > 2 \cap LBP_{P,R} \in LB^{dnu} \\ P+1+K_{\sigma}^{riu2}, & U(LBP_{P,R}) > 2 \cap LBP_{P,R} \notin LB^{dnu} \end{cases} \quad (8)$$

where $K_{\sigma}^{riu2} \leq K_{\sigma}$, it is the total number of the rotation invariant pattern codes for the trained $LB^{dnu}[1, \dots, K_{\sigma}]$ according to (3).

$$SDLBP_{P,R}^{hriu2ln} = \begin{cases} \sum_{i=0}^{P-1} s(g_p - g_c), & U(LBP_{P,R}) \leq 2 \\ \{P+1, \dots, P+K_{\sigma}^{ln}\}, & U(LBP_{P,R}) > 2 \cap LBP_{P,R} \in LB^{dnu} \\ P+1+K_{\sigma}^{ln}, & U(LBP_{P,R}) > 2 \cap LBP_{P,R} \notin LB^{dnu} \end{cases} \quad (9)$$

where K_{σ}^{ln} is the number of the condensed DNUPs by only replacing σ with $\sigma' = \eta_{PSNR} \times \sigma$ in Algorithm 1, and the $\eta_{PSNR} \leq 1$ is the ratio of the average *peak signal to noise ratio* (PSNR) of degraded images to that of their standard training images. Hence, the mapped labels are composed of three consecutive parts: $P+1$ of rotation invariant uniform patterns, K_{σ}^{riu2} or K_{σ}^{ln} DNUPs for 'hriu2' or 'hriu2ln', and one miscellaneous remainder pattern. Intuitively, the two kinds of hybrid lookup tables have 2^P elements, generating $P+2+K_{\sigma}^{riu2}$ or $P+2+K_{\sigma}^{ln}$ histogram atoms. This configurations support distinct industrial applications i.e., the former with

Algorithm 1 Searching the dominant non-uniform patterns of SDLBP

Training image set, $T = \{t_i [r \times c] \mid i=1, 2, \dots, N\}$, constituted of N image samples with a size of $r \times c$ pixels, the targeted proportion of total selected patterns, τ , and the predefined binary length P and neighborhood radius R .

Input:

Output: K_{σ} dominant non-uniform pattern labels, $LB^{dnu}[1, \dots, K_{\sigma}]$

Main procedure:

1. Initialize two $(r-2R) \times (c-2R)$ zero matrixes L^{u2} and L^{nu} for keeping the uniform and non-uniform pattern labels, and two 1×2^P zero arrays H^{u2} and H^{nu} for keeping the corresponding histograms of L^{u2} and L^{nu} .
2. **FOR** each image t_i in the training image set T
3. **FOR** each center pixel $g_c, (j_r, j_c) \in t_i, j_r=1, \dots, (r-2R)$, and $j_c=1, \dots, (c-2R)$
4. Calculate each LBP pattern label $L_{i, (j_r, j_c)}$ of g_c based on $LBP_{P,R}^{riu2}$ (1)
5. **IF** $U(L_{i, (j_r, j_c)}) \leq 2$
6. Update the uniform pattern matrix: $L_{i, (j_r, j_c)}^{u2} = L_{i, (j_r, j_c)}$
Increase the number of the corresponding label: $H^{u2}[LBP_{P,R}]++$
7. **ELSE IF** $U(L_{i, (j_r, j_c)}) > 2$
8. Update the non-uniform pattern matrix: $L_{i, (j_r, j_c)}^{nu} = L_{i, (j_r, j_c)}$
Increase the number of the corresponding label: $H^{nu}[LBP_{P,R}]++$
9. **END IF**
10. **END FOR**
11. **END FOR**
12. Sort the histogram H^{nu} in descending order.
Calculated P_{sup} , which is the number ratio: $H^{nu} / (H^{u2} + H^{nu})$.
Update threshold σ according to (7).
13. Find the number of the front pattern occurrences K_{σ} according to the following inequality, and then store the corresponding pattern labels into the dominant non-uniform label tank $LB^{dnu}[1, \dots, K_{\sigma}]$.

$$K_{\sigma} = \arg \min_k \left(\frac{\sum_{k=1}^{K_{\sigma}} H^{nu}(k)}{\sum_{k=1}^{2^P} H^{nu}(k)} \geq \sigma \right), \sigma \in [0, 1]$$

14. Return K_{σ} and the selectively dominant pattern labels $LB^{dnu}[1, \dots, K_{\sigma}]$.

Algorithm 2 Extracting a SDLBP histogram feature vector

Input: A training or testing image $I[r \times c]$, and the pre-learned $LB^{dnu}[1, \dots, K_{\sigma}]$.

Output: The feature vector of image I based on $SDLBP_{P,R}^{hriu2}$.

Main procedure:

1. Initialize the hybrid pattern histograms $SDPH^{hriu2}[1, \dots, (P+2+K_{\sigma}^{riu2})]=0$.
2. **FOR** each image in the given image sample I
3. **FOR** each center pixel $g_c, (j_r, j_c) \in I, j_r=1, \dots, (r-2R)$, and $j_c=1, \dots, (c-2R)$
4. Calculate each LBP pattern label of g_c based on $SDLBP_{P,R}^{hriu2}$ (8)
5. Increase the corresponding histogram bin: $SDPH^{hriu2}[LBP_{P,R}]++$
6. **END FOR**
7. **END FOR**
8. Return $SDPH^{hriu2}[1, \dots, (P+2+K_{\sigma}^{riu2})]$ as the feature vector of SDLBP for I .

abundant DNUPs targets full-extraction while the latter with lightweight K_{σ}^{ln} targets noise avoidance.

C. Feature Extraction Scheme

The pseudo codes for feature extraction using the proposed $SDLBP_{P,R}^{hriu2}$ are given in Algorithm 2. First, an array with a

size of $1 \times (P+2+K_{\sigma}^{ri})$ is initialized for keeping the hybrid pattern histograms. Then, for each image in the given image set, a matrix with a size of $(r-2R) \times (c-2R)$ maintains the calculated $SDLBP_{P,R}^{hriu2}$ codes of its each center pixel, the corresponding histogram bins are updated during the same loop. Finally, the updated histogram $SDPH^{hriu2}$ is returned as the feature vector. Similarly, we can easily obtain the $SDPH^{hriu2ln}$ by replacing the mapping scheme in Algorithm 2 with $SDLBP_{P,R}^{hriu2ln}$ if necessary.

Two **generalized properties** of $SDLBP_{P,R}^{hriu2}$ which are important to highlight are; firstly, the LBP operator on the line 4 of Algorithm 1 is not limited to the $LBP_{P,R}^{orig}$, descriptors such as CLBP [17], or local ternary patterns (LTP) [31], etc. and can be improved through our SDLBP framework, thus generating variants of SD-CLBP, SD-LTP etc. Secondly, the proposed $SDLBP_{P,R}^{hriu2}$ inherits the functions of $LBP_{P,R}^{orig}$ perfectly. Concretely, the $SDLBP_{P,R}^{hriu2}$ operator could transmute itself into the operators of $LBP_{P,R}^{riu2}$ or $LBP_{P,R}^{ri}$ when the ratio threshold of pattern occurrence (σ) is set to 0 or 1, respectively.

D. Multi-region Histogram and Feature Matching

Generally, the regions of defects are much smaller than their resident steel surfaces [6]. Adopting LBP operators to whole images would lead to spatial information degeneration on regional level, the chain reaction is that the classification accuracy will be pulled down by the active steel textures and/or potential pseudo-defects.

For this consideration, the multi-region analysis method [19] is imported as a reference for the defect representation of steel surface. The corresponding calculations in the Algorithm 1 and Algorithm 2 are then applied to m non-overlapping separated regions of testing image samples. The final feature vectors are combined as

$$SDPH_{i,j}^R = \sum_{x,y} f\{I(x,y)=i\} f\{(x,y) \in R_j\}, f(z) = \begin{cases} 1, & z \text{ is true} \\ 0, & z \text{ is false} \end{cases} \quad (10)$$

where $i=0,...,P+1+K_{\sigma}^{ri}$ (or $P+1+K_{\sigma}^{in}$) and $j=0,...,m-1$ are the label and region indexes, respectively, and (x, y) are the pixel coordinates among a designated image region.

In this work, the nearest neighbor classifier (NNC) is selected as the dissimilarity metric between two multi-region histograms, a test sample \mathbf{T} to be matched will be appointed to the class model \mathbf{M} if it occupies the minimum chi-square distance

$$\chi_w^2(\mathbf{T}, \mathbf{M}) = \sum_{i,j} \omega_j \frac{(T_{i,j} - M_{i,j})^2}{T_{i,j} + M_{i,j}}, \begin{cases} i \in [0, P+1+K_{\sigma}^{ri} \text{ (or } P+1+K_{\sigma}^{in})] \\ j \in [0, m-1] \end{cases} \quad (11)$$

where $T_{i,j}$ and $M_{i,j}$ are respectively the values of the test sample and the trained image at the i^{th} bin of the j^{th} region, and ω_j is the weight of j^{th} region. Conversely, the facial outlines and features are relatively fixed, the type, size, number, as well as location of steel surface defects are arbitrary. Thus, the region weight ω_j can not be manually set like face recognition. To address the above problems, an adaptive region weighting (ARW) method is developed

$$\omega_j = ROOF \left\{ \frac{1}{s_g} \sum_{x,y} \{g_j(x,y)\}^2 - \left\{ \frac{1}{s_g} \sum_{x,y} g_j(x,y) \right\}^2 \right\}, j \in [0, m-1] \quad (12)$$

where $g_j(x, y)$ denotes the pixel gray value of the (x, y) coordinates in the j^{th} region, the $s_g=r_g \times c_g$ is the size of the image region, which is recommended to be set as 32 pixel \times 32 pixel, and the $ROOF(\cdot)$ is a normalization operator. Intuitively, the more informative areas (i.e., edges, spots), the bigger the variances, then the higher the region weights. An example of this is shown in Fig. 1(b), where an intuitive explanation is offered for the defect image. As shown in the Fig. 2(c), the brighter square indicates that a higher region weight will be assigned.

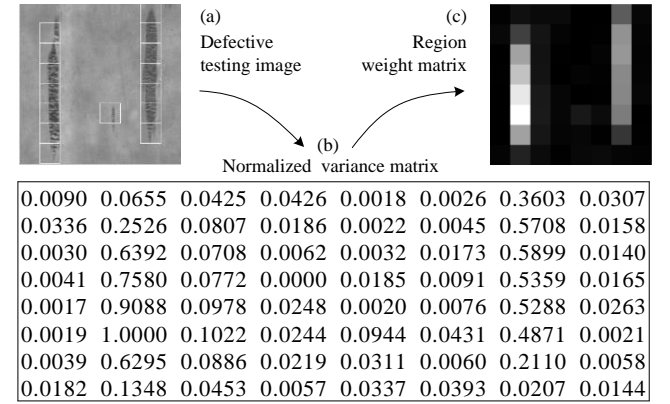


FIGURE 2. Brief illustration of the adaptive region weighting mechanism.

TABLE I
TEXTURE TEST SUITES AND IMPLEMENTATION DETAILS

Information	TC10	TC12
Illumination types	'Inca'	'Inca', 'Horizon', 'TL84'
	0, 5, 10, 15, 30, 45, 60, 75,	
Rotations (°)	90	0
Image resolution	128 × 128 pixel	128 × 128 pixel
Image number	4320	1440
Class number	24	24
Train image number	480 (20 × 24, 0°, 'Inca')	480 (20 × 24, 0°, 'Inca')
Test image number	3840 (8 × 20 × 24)	960 (2 × 20 × 24)

IV. EXPERIMENTS AND DISCUSSIONS

This section provides diverse experiments and comparative analyses. First, with an instantiation of SD-CLBP, extensive tests on a widely used textile texture database (Outex [29]) are carried out to evaluate the SDLBP framework. Second, the overall performances of SDLBP scheme are verified on an actual surface defect database (Dragon [30]) captured from real-world hot-rolled steel strips [6].

A. Experimental Results on Outex Database

1) TEXTURE SUITES AND IMPLEMENTATION DETAILS

Similar to the experimental setups in [15] [17] [18], two commonly used test suites of Outex_TC_00010 (TC10) and Outex_TC_00012 (TC12) are selected for the performance evaluation of SDLBP. (They can be downloaded from the URL: <http://lagis-vi.univ-lille1.fr/datasets/outex.html>). As illustrated in TABLE I, the two test suites include the same

24 classes of textures, which are captured under 3 different illuminations ('Inca', 'Horizon', and 'TL84') and 9 distinct rotation angles (0°, 5°, 10°, 15°, 30°, 45°, 60°, 75°, and 90°). Generally, TC10 and TC12 focus on the rotation invariance and the illumination robustness, respectively.

2) RESULTS AND ANALYSIS

We discuss our testing results in *seven* diverse respects.

a) Dominant Pattern Threshold (σ) Verification. We carried out a series of tests to verify a suitable interval of the threshold σ on the illumination-aware TC12. Under normal image quality conditions ($\eta_{PSNR}=1$), Fig. 3 exhibits the classification accuracy rates of the 7 SD-CLBP variants under 11 evenly spaced thresholds by using 2 different classifiers. For visual comparison, the results of the original $CLBP_{P,R}^{riu2}$ and $CLBP_{P,R}^{ri}$ are presented on both sides as baselines. From Fig. 3(a), regardless of the value of σ , nearly all the $SD-CLBP_{P,R}^{riu2}$ variants yield higher accuracy rates than both $CLBP_{P,R}^{riu2}$ and $CLBP_{P,R}^{ri}$. Intuitively, for a certain operator, its scores first experience a continuous rise, then achieve to a maximum, finally fall back gradually to the score of $CLBP_{P,R}^{ri}$, which precisely prove that the remainder non-uniform patterns are extremely difficult to estimate. From our experiments, an interval of 0.4~0.6 (in practice, set to 0.5) for σ could cover more than 90% of pattern proportion, which is also consistent with the analysis presented in Sec. II.B and the empirical parameter drawn in DLBP [18].

b) Classification Accuracy. Since SD-CLBP completely preserves the properties of CLBP, we take a very representative descriptor (SD-CLBP_S/C) for an example. As shown in Fig 3, when $\tau=90\%$ and classifier=ARW-NNC, the $SD-CLBP_{S,8,1}^{riu2}/C$ wins a score of 96.99%, it is competitive with 95.11% of $CLBP_{S,8,1}^{riu2}/C$ and 96.01% of $CLBP_{S,8,1}^{ri}/C$. With the same conditions, the $SD-CLBP_{S,8,1}^{riu2ln}/C$ promotes its score to 98.46%. Theoretically, bigger P and R could obtain better performance. The preliminary results prove our SDLBP methodology achieves considerable improvements, even with the roughest coverage area of $(P,R)=(8,1)$.

c) Noise Avoidance. Interestingly, as shown in Fig. 3(b), the $SD-CLBP_{S,8,1}^{riu2ln}$ performs even better than $SD-CLBP_{S,8,1}^{riu2}$ without regard for rotation invariance of DNUPs, especially when σ exceeds 0.5, which can reserve more margin to resist noise. However, the related time-efficiency (refer to Fig. 4) would degenerate dramatically owing to the feature dimension expansion. That is why we restrict K_{σ}^{in} to a lower level in (9), which is a compromise between the classification accuracy and the runtime overhead. In this work, if image quality declines, $SDLBP_{P,R}^{riu2ln}$ will not be enabled until η_{PSNR} is no more than 0.9. Then less DNUPs would be extracted adaptively. This simple convertible mechanism benefits to both noise avoidance and time-efficiency. Consequently, the proposed $SDLBP_{P,R}^{riu2ln}$ offers a better alternative for anti-noise, how to consummate its theory for widely application will be our future work.

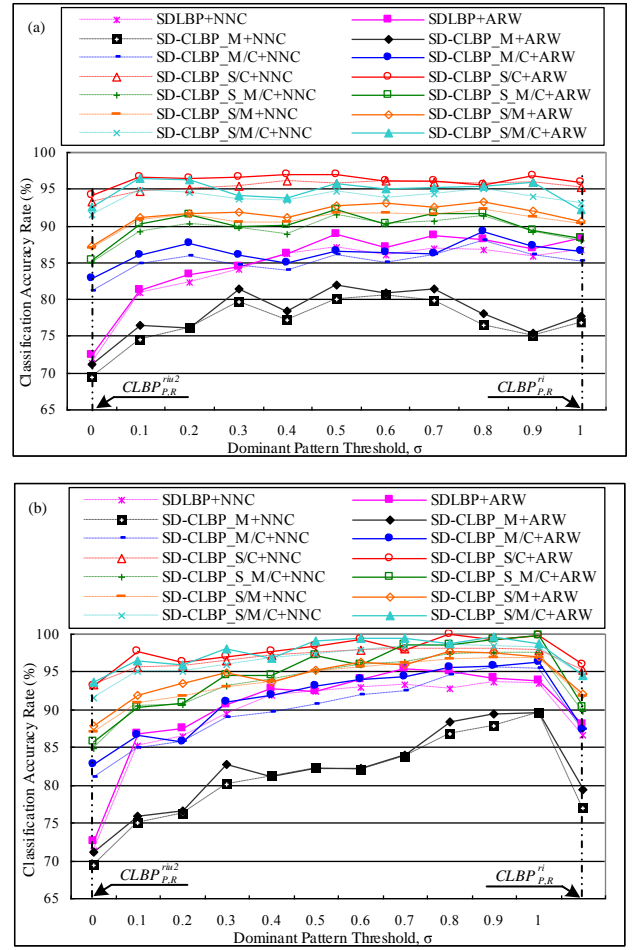


FIGURE 3. Classification accuracy rates on TC12 using (a) $SD-CLBP_{P,R}^{riu2}$, (b) and $SD-CLBP_{S,8,1}^{riu2ln}$, where “ARW” denotes “ARW-NNC”.

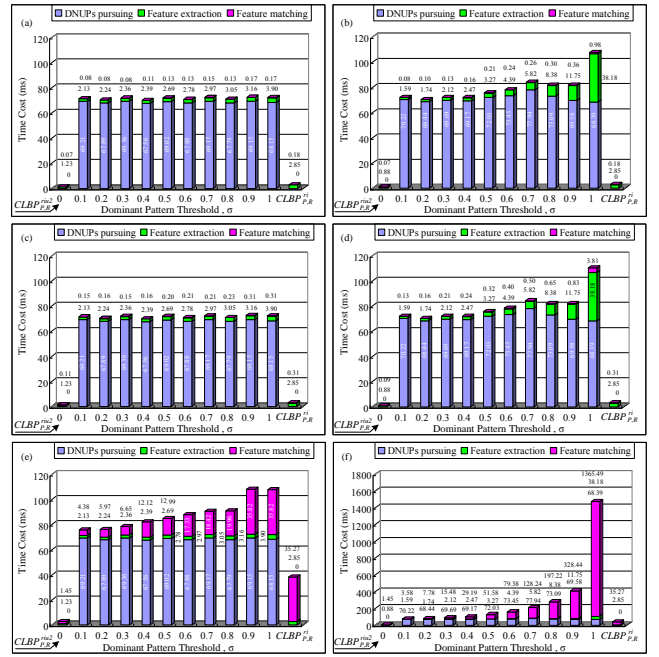


FIGURE 4. Classification time costs using (a) $SD-CLBP_{P,R}^{riu2}$, (b) $SD-CLBP_{S,8,1}^{riu2ln}$, (c) $SD-CLBP_{S,8,1}^{riu2}/C$, (d) $SD-CLBP_{S,8,1}^{riu2ln}/C$, (e) $SD-CLBP_{S,8,1}^{riu2ln}/M_{8,1}$, and (f) $SD-CLBP_{S,8,1}^{riu2ln}/M_{8,1}/C$, all the variants operate with ARW-NNC.

d) Performance of ARW-NNC. Testing results in Fig. 3 indicate the ARW-NNC performs better than its foundational NNC, with an around 1% but reliable increase on classification accuracy. This improvement is also can be observed in TABLE III, the scores of $ICLBP_{P,R}^{hriu2}$ are slightly lower than those of $SD-CLBP_{P,R}^{hriu2}$ by around 0.6%, while the only difference between them is whether they have used ARW scheme to improve the NNC. The reason of the mediocre improvement is that the universal homomorphism of the texture images make it is difficult to obtain discriminative regional variances. However, for the steel surface images, due to their remarkable line singularity, the ARW-NNC is expected to achieve more significant promotion, which will be discussed in Section IV.B.

e) Time-Efficiency. To simplify the layout, Fig. 4 evaluates the time-efficiency by contrasting the runtime overheads of only three pairs of typical $SD-CLBP_{8,1}^{hriu2}$ and $SD-CLBP_{8,1}^{hriu2ln}$ variants. The measuring was carried out on Matlab R2010a, with an Intel CPU (E3-1230-v5, 3.4 GHz) and 8G RAM. In addition, all the results are normalized to the average time per image. Generally, given certain P and R , the runtime overheads for DNUPs pursuing are independent with SD-CLBP variant types. This training time is within 80 ms, but is required only once. The actual classification time costs are spent on feature extraction and feature matching. In particular, given $\sigma=0.5$, the classification time of $SD-CLBP_{8,1}^{hriu2}/C$ is only 2.89 ms (2.69 ms for feature extraction, and 0.20 ms for feature matching), which is better than $CLBP_{8,1}^i/C$ (3.16 ms) while slightly worse than $CLBP_{8,1}^{riu2}/C$ (1.34 ms). But this negligible extra time brings 2.88% score increase over $CLBP_{8,1}^{riu2}/C$ (from 94.11% to 96.99%).

When it comes to $SD-CLBP_{8,1}^{hriu2ln}$, the runtime costs spent on feature extraction and matching all present an upward trend with the increase of σ . Concretely, the former increase trend is relatively mild when $\sigma \leq 0.8$, but the latter one is quite notable, especially in Fig. 4(f). Nevertheless, the variants in Fig. 4(b) and Fig. 4(d) with $\sigma \leq 0.6$ are still comparable to those of $SD-CLBP_{8,1}^{hriu2}$. In practice, the $SD-CLBP_{P,R}^{hriu2ln}/C$ variants with smaller σ (≤ 0.4) are highly recommended for anti-noise applications, but the $SD-CLBP_{P,R}^{hriu2ln}/M_{P,R}^{hriu2ln}/C$ does not.

f) Multi-resolution Configurations. According to [15], multi-resolution histogram matching by employing multiple operators with distinct (P, R) can improve classification accuracy. As illustrated in TABLE II, among the four approaches of single-resolution, the descriptors with parameter of $(P,R)=(8,3)$ win more balanced performance, achieving competitive scores (94.46% for $SDLBP_{8,3}^{hriu2}$, and 98.97% for $SD-CLBP_{8,3}^{hriu2}/C$), but requiring nearly the smallest feature dimension (only 29). Regarding to the multi-resolution groups, $SD-CLBP_{8,3}^{hriu2}/C$ performs slightly better than $SD-CLBP_{8,3}^{hriu2}/C$, with a negligible promotion of less than 0.5%, but the feature dimension is nearly doubled (from 351×2 to 563×2). Consequently, the

configurations of $(P,R)=(8,3)$ and $(P,R)=(8,1)+(8,3)+(16,2)$ are recommended for single- and multi-resolution scheme, respectively.

g) Comparative Evaluation. In order to avoid changing configurations to preserve fair comparison, all participant results for the proposed $SDLBP_{P,R}^{hriu2}$ are gathered from TABLE II (marked with gray background). TABLE III presents the comparative classification performance with those of other twelve recent state-of-the-art LBP variants on TC10 and TC12. Besides, we listed the scores of two of our GCLBP-based variants ($ICLBP$, $ICLBP_{S/C}$) for contrast. For the twelve competitors, even the fundamental $SDLBP_{P,R}^{hriu2}$ ($SD-CLBP_{P,R}^{hriu2}$) scheme has effortlessly outweighed the other eight methods. For the remainder four winners, the feature sizes of $CLBP_{P,R}^{riu2}/M_{P,R}^{riu2}/C$ and $dis(S+M)_{P,R}^{riu2}$ are far larger than our $SDLBP_{P,R}^{hriu2}$. Fortunately, the time efficiency had drawn increasing attentions in the new developed COV-LBPD and $MRELBP_{P,R}^{num}$. Nevertheless, our method still holds the advantage in this aspect. It can be clearly learnt that $SD-CLBP_{P,R}^{hriu2}/C$ adapting multi-resolution scheme works consistently better than the first twelve methods in classification scores, while its feature size is competitive to others at most of the time. It is worth noting that the scores of $MRELBP_{P,R}^{num}$ here are slightly lower than those in [21], the main reason is that we use NNC to replace its previous SVM for fair comparison in this paper. In particular, from TABLE II and TABLE III, if using a certain condition of $(P, R)=(8, 3)$, the score is boosted from 85.51% of $CLBP_{S+NNC}$ to 93.60% of $ICLBP+NNC$, where $ICLBP$ is essentially a special case of $SD-CLBP_{S}$. This improved score (93.60%) is promoted to 94.46% of $SD-CLBP_{S+ARW-NNC}$ once again. These results prove that the SDLBP framework itself plays a leading role while the ARW-NNC scheme plays only a supplementary role in improving classification accuracy.

B. Overall Performance on Dragon Database

1) COMPARED METHODS AND EVALUATION SETUP

In this section, we continue to use SD-CLBP to evaluate the classification accuracy and runtime overhead of the SDLBP scheme on a real-world steel surface defect database, Dragon [30]. Several typical methods of LBP/VAR [15], DLBP [18], CLBP [17], LTP [31], MRELBP[21], ICLBP_S/C [26] and AECLBP [7] are selected for extensive comparison. To be fair, all the descriptors choose the same NNC series classifiers, we continue use the parameter settings in TABLE III, i.e., $SDLBP_{8,1+8,3+16,4}^{hriu2}$ and $SD-CLBP_{8,1+8,3+16,4}^{hriu2}/C$ with $\tau=90\%$, and the other competitors are configured with the best-fit parameters claimed by their authors, i.e., $LBP_{8,1+16,2+24,3}^{riu2}/VAR_{8,1+16,2+24,3}$, $DLBP_{24,3}^{riu2}$ with 80% dominant pattern proportion, $CLBP_{8,1+16,2+24,3}^{riu2}/M_{8,1+16,2+24,3}^{riu2}/C$, $LTP_{8,1+16,2+24,3}^{riu2}$, $MRELBP_{8,1+8,3+8,5+8,7}^{num}$, $AECLBP_{8,1+16,2+24,3}^{riu2}/M_{8,1+16,2+24,3}^{riu2}/C$. Our $SD-CLBP$ and $ICLBP_{S/C}$ descriptors adopt smaller scope of multi-resolution scheme than others because ours show better performance than others even with lower configurations.

TABLE II
ACHIEVED CLASSIFICATION ACCURACY RATES (%) OF THE PROPOSED SD-CLBP ON TC10 AND TC12 WHEN $\sigma=0.5$, AND MAPPING SCHEME OF 'HRIU2'

(P,R)	(8,1)				(8,3)				(16,2)				(16,4)			
	TC10	tl84	horizon	Mean	TC10	tl84	horizon	Mean	TC10	tl84	horizon	Mean	TC10	tl84	horizon	Mean
LBP (CLBP_S)+ NNC [15]	84.81	72.34	70.36	75.84	86.12	85.74	84.68	85.51	88.96	84.32	80.88	84.72	96.46	87.52	86.02	90.00
CLBP_S/C + NNC [17]	92.53	94.12	92.54	93.06	94.52	94.45	93.25	94.07	96.93	92.65	91.11	93.56	98.85	93.53	92.73	95.04
SDLBP (SD-CLBP_S)+ARW-NNC	89.06	88.77	88.79	88.87	87.12	98.69	97.56	94.46	93.63	92.09	91.66	92.46	94.80	97.77	96.64	96.40
SD-CLBP_S/C + ARW-NNC	97.07	97.25	96.72	97.01	97.66	99.80	99.45	98.97	98.16	98.13	97.91	98.07	99.90	99.04	99.52	99.49
Total number of the dominant patterns	23				29				212				299			
(P,R)	(8,1) + (8,3)				(8,1) + (8,3) + (16,2)				(8,1) + (8,3) + (16,4)				(8,1) + (8,3) + (16,2) + (16,4)			
	TC10	tl84	horizon	Mean	TC10	tl84	horizon	Mean	TC10	tl84	horizon	Mean	TC10	tl84	horizon	Mean
LBP (CLBP_S) + NNC [15]	86.05	72.08	71.44	76.52	86.27	86.28	84.62	85.72	96.24	87.43	86.48	90.05	97.52	87.60	86.16	90.43
CLBP_S/C + NNC [17]	93.11	95.69	93.40	94.07	94.53	94.37	93.16	94.02	98.93	94.21	92.58	95.24	99.75	93.66	92.55	95.32
SDLBP (SD-CLBP_S)+ARW-NNC	88.88	89.09	90.10	89.35	90.19	98.88	97.67	94.58	95.02	98.31	97.28	96.87	97.12	99.79	97.39	97.77
SD-CLBP_S/C + ARW-NNC	98.22	96.86	97.03	97.37	97.53	99.79	99.36	98.89	99.75	98.96	99.63	99.45	99.94	99.32	99.98	99.75
Total number of the dominant patterns	52				264				351				563			

TABLE III
COMPARING THE CLASSIFICATION ACCURACY RATES (%) ACHIEVED BY OUR PROPOSED SD-CLBP WITH THOSE OF RECENT STATE-OF-THE-ART METHODS

Method		TC12				Feature dimension
		TC10	tl84	horizon	Mean	
$SDLBP_{P,R}^{hri2}$	Single-resolution	87.12	98.69	97.56	94.46	29
	Multi-resolution	95.02	98.31	97.28	96.87	351
$SD-CLBP_{P,R}^{hri2}/C$	Single-resolution	97.66	99.80	99.45	98.97	58
	Multi-resolution	99.75	99.96	99.63	99.45	702
$ICLBP_{P,R}^{hri2}$ [26]	Single-resolution	86.22	97.66	96.92	93.60	29
	Multi-resolution	95.61	96.68	95.86	96.05	351
$ICLBP_{P,R}^{hri2}/C$ [26]	Single-resolution	96.93	99.09	99.25	98.42	58
	Multi-resolution	99.59	99.33	99.21	99.38	702
$LBP_{P,R}^{m2}/VAR_{P,R}$ [15]		97.87 ^a	88.42 ^a	86.79 ^a	91.02 ^a	864
$DLBP$ [18]		98.52 ^a	93.65 ^a	91.47 ^a	94.55 ^a	37
$CLBP_{P,R}^{m2}/M_{P,R}^{m2}/C$ [17]		99.14 ^b	97.60 ^b	98.98 ^b	98.57 ^b	2200
$LTP_{P,R}^{m2}$ [31]		98.62 ^a	92.05 ^a	91.59 ^a	94.09 ^a	108
$CLBC$ [32]		98.96	95.37	94.72	96.35	1990
$dis(S+M)_{P,R}^{m2}$ [33]		98.93	97.00	96.50	97.48	2668
$NTLBP_{P,R}^{faith}$ [34]		99.24	96.18	94.28	96.57	108
$NRLBP_{P,R}^{m2}$ [35]		93.44	96.13	87.38	88.98	30
$MSJLBP$ [36]		96.67	95.21	95.74	95.87	3540
$PRICoLBP_s$ [37]		94.48	92.57	92.50	93.18	3540
$COV-LBPD$ [38]		98.78	95.72	97.62	97.37	289
$MRELBP_{P,R}^{nm}$ [21]		99.87^a	99.49^a	99.75^a	99.70^a	800

^aThese results are obtained from our own implementation, ^bThese results are obtained from our implementation but by using the open codes from the authors.

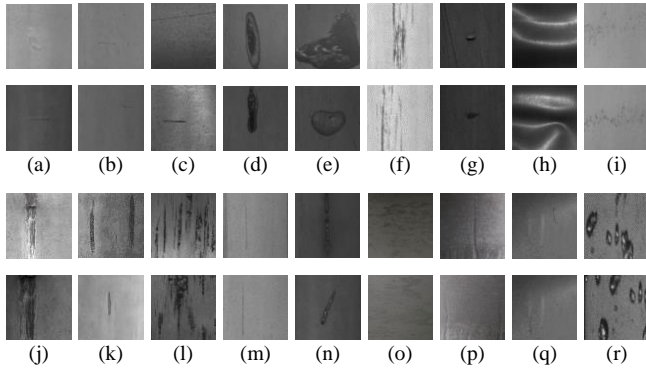


FIGURE 5. The 18 classes of steel surface defects on Dragon_Valin_TS01: (a) Roll mark, (b) horizontal crackle, (c) horizontal scratch, (d) entrapped slag, (e) heavy swelling, (f) longitudinal scar, (g) hole, (h) shape wave, (i) hard spots, (j) sharp scarring, (k) oxide scale, (l) Skin lamination, (m) longitudinal tiny scratch, (n) unexpected inclusion, (o) horizontal double skin, (p) multiple wrinkle, (q) longitudinal crack, and (r) water drops.

'Dragon' is a steel surface defect database captured from actual hot-rolling lines [30]. To verify our methods, we selected one test suite (Dragon_Valin_TS01) collected in Valin LY Steel [6] for performance evaluation. It contains 18 classes of defects, each class includes 300 non-overlapping samples, and each image sample has a resolution of 256 pixel \times 256 pixel. During the test, 1080 (18 \times 60) randomly selected samples from the 18 classes are used for classifier training and the other 4320 (18 \times 240) samples are used for testing. Fig. 5 exhibits 18 \times 2 defect samples for descriptive visual sense. It can be clearly observed that the classification task is extremely challenging as declared in Section I.

2) RESULTS AND DISCUSSION

The average experimental figures carried out on the test suite of Dragon_Valin_TS01 are listed in TABLE IV. As expected, ARW-NNC scheme significantly promotes the

classification rates of our SDLBP with NNC. Compared with DLBP and LTP, our basic *SDLBP* with ARW-NNC performs better but with a litter bit more runtime overheads. This score is even roughly the same as that of *CLBP_S/M/C* (94.68% vs. 94.59%). While the runtime overhead is quite competitive than that of *CLBP* (73.36 ms vs. 266.92 ms). Interestingly, with more lightweight configurations, the score of our *SD-CLBP_S/C* with the same NNC is even slightly ahead of the *CLBP_S/M/C* (94.93% vs. 94.59%). This contrast result firmly proves that the descriptive information implicitly existing among the non-uniform patterns are indeed benefit to defect classification. Further, the noise robust *AECLBP_S/M/C* promotes the score of *CLBP_S/M/C* from 94.59% to 95.07%, however, the time cost is higher than its original *CLBP_S/M/C*, since it needs to pay extra time on adjacent evaluation for center pixels. When using ARW-NNC, our *SD-CLBP_S/C* yields a considerable score of 97.62% with an acceptable time cost of about 0.10 s. In addition, the score of *MRELBP* is not as remarkable as before (TABLE III), we think the main reasons are the adopted simpler NNC (vs. SVM) and the more challenging defect classification task (vs. texture classification task). The slightly higher score of *SD-CLBP_S/C* compared with *ICLBP_S/C* mainly benefits from the adopted ARW-NNC. And the relatively high runtime overheads of *CLBP* and *AECLBP* mainly result from the multi-resolution scheme with a wide scale of (8,1)+(16,2)+(24,3).

3) ANTI-NOISE METHODOLOGY EXPLORATION

Here, we present the preliminary study to how to choose the encoding schemes for anti-noise. As shown in Fig. 6, according to different η_{PSNR} , we define *three* states for steel surface AOI instruments: normal state ($0.9 < \eta_{PSNR} \leq 1$), early-warning state ($0.75 \leq \eta_{PSNR} \leq 0.9$), and serious alarm state ($\eta_{PSNR} < 0.75$).

1) Under the first state, the coding scheme of 'hriu2' is highly recommended. Refer to the left side of Fig.6, compared to drastically sacrifice time efficiency ($\eta_{PSNR}=1$: feature dimension, 70 vs. 29), we prefer to undertake minor compromise of accuracy ($\eta_{PSNR}=1$: 94.69 vs. 94.17).

2) Under the second state, since the rotation invariance of non-uniform patterns degenerates gradually with the decrease of image quality, the classification accuracy of *SD-CLBP_S^{hriu2}/C* decrease significantly. To address this problem, we suggest to convert to the coding scheme of 'hriu2ln'. And the runtime overhead could be acceptable ($\eta_{PSNR}=0.8$: feature dimension, 30 vs. 29) because the feature dimensions have been restricted to a large extent in (9).

3) The last state is not allowed to the AOI instruments, which will trigger emergency alarm. In fact, at the second stage, the AOI instrument will continuously send out early-warning signals, reminding operators to investigate the potential failures of related equipments (i.e., optical devices, image acquisition cards, rollers, optical-fiber cables, etc.).

TABLE IV
COMPARING THE OVERALL PERFORMANCE OF OUR SDLBP WITH THOSE OF THE RECENT STATE-OF-THE-ART METHODS ON DRAGON_VALIN_TS01

Method		Dragon-TS01	
LBP operator	Classifier	Score (%)	Classification time (ms)
<i>SDLBP_{P,R}^{hriu2} (SD-CLBP_S^{hriu2})</i>	NNC	87.55	71.93
	ARW-NNC	94.68	73.36
<i>SD-CLBP_S^{hriu2}/C</i>	NNC	94.93	90.29
	ARW-NNC	97.62	100.08
<i>LBP_{P,R}^{hriu2}/VAR_{P,R}</i> [15]	NNC	88.26	110.73
<i>DLBP_{P,R}^{hriu2}</i> [18]	NNC	91.14	46.45
<i>CLBP_S^{hriu2}/M_{P,R}^{hriu2}/C</i> [17]	NNC	94.59	266.92
<i>LTP_{P,R}^{hriu2}</i> [31]	NNC	90.37	68.57
<i>MRELBP_{P,R}^{hriu2}</i> [21]	NNC	96.32	176.86
<i>ICLBP_S/C</i> [26]	NNC	96.54	82.51
<i>AECLBP_S^{hriu2}/M_{P,R}^{hriu2}/C</i> [7]	NNC	95.07	309.38

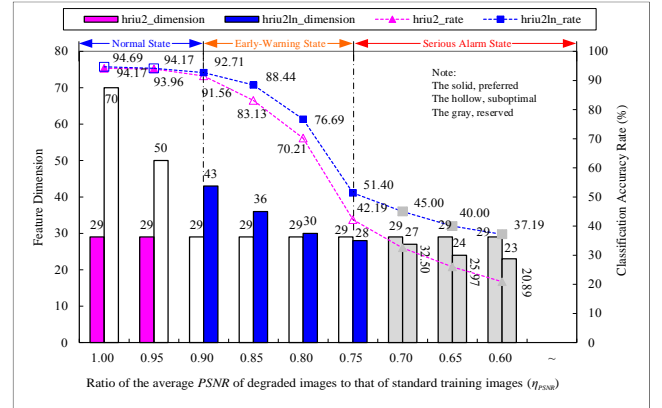


FIGURE 6. Coding-convertible working mechanism and its noise-avoidance effect. (Measuring conditions: *SD-CLBP_S^{hriu2}/C*, *SD-CLBP_S^{hriu2ln}/C*, $\sigma=0.5$, NNC.)

To sum up, our SDLBP framework has achieved balanced performance between classification accuracy and time efficiency for surface defect inspection of steel strips, various variants could be flexibly obtained for different applications.

V. CONCLUSION

Herein, we have proposed a new SDLBP framework to enhance comprehensive performance of current LBP variants in both classification accuracy and time efficiency. On a widely used texture database, the SDLBP descriptors achieved nearly perfect results, outperforming recent state-of-the-art LBP-like descriptors. While on a fresh surface defect database obtained from real-world hot-rolling mills, the fundamental *SDLBP_{P,R}^{hriu2} (SD-CLBP_S^{hriu2})* and improved *SD-CLBP_S^{hriu2}/C* achieved classification scores of 94.68% and 97.62% respectively. And the required average runtime overheads are both within 0.10s. These actual achievements promise that the proposed SDLBP framework could be applied to many manufacturing industries with time-limited condition but high-accuracy requirement, not limited to the sheet materials like hot-rolled steel strips.

Future works will concentrate on two aspects. 1. To develop sparser model for representing the DNUPs, then more compact feature vectors would be obtained for

reducing the computational loads of classifiers. 2. To optimize the code for large surface images and implement the proposed method on FPGA to improve parallelizability.

REFERENCES

- [1] X. Wen, K. Song, K. M. Niu, Z. Dong and Y. Yan, "A three-dimensional inspection system for high temperature steel product surface sample height using stereo vision and blue encoded patterns," *Optik*, vol. 38, pp. 131–148, Apr. 2017.
- [2] P. C.-Solly and J. E. Smith, "Adaptive surface inspection via interactive evolution," *Image Vis. Comput.*, vol. 25, no. 7, pp. 1058–1072, Jul. 2007.
- [3] S. Ghorai, A. Mukherjee, M. Gangadharan, *et al.* "Automatic defect detection on hot-rolled flat steel products," *IEEE Trans. Instrum. Meas.*, vol. 62, no. 3, pp. 612–621, Mar. 2013.
- [4] S. Ghorai, A. Mukherjee and P. K. Dutta, "Discriminant analysis for fast multiclass data classification through regularized kernel function approximation," *IEEE Trans. Neural Netw.*, vol. 21, no. 6, pp. 1020–1029, Jun. 2010.
- [5] K. Liu, H. Wang, H. Chen, *et al.* "Steel surface defect detection using a new Haar-Weibull-Variance model in unsupervised manner," *IEEE Trans. Instrum. Meas.*, vol. 66, no. 10, pp. 2585–2596, Oct. 2017.
- [6] Q. Luo and Y. He, "A cost-effective and automatic surface defect inspection system for hot-rolled flat steel," *Robot. Comput.-Integr. Manuf.*, vol. 38, pp. 16–30, Apr. 2016.
- [7] K. Song and Y. Yan, "A noise robust method based on completed local binary patterns for hot-rolled steel strip surface defects," *Appl. Surf. Sci.*, vol. 285, no. 21, pp. 858–864, Nov. 2013.
- [8] Y. Park and I. S. Kweon, "Ambiguous surface defect image classification of AMOLED displays in smartphones," *IEEE Trans. Ind. Informat.*, vol. 12, no. 2, pp. 597–607, Jan. 2016.
- [9] R. Usamentiaga, D. F. Garcia, J. Molleda, *et al.* "Vibrations in steel strips: effects on flatness measurement and filtering," *IEEE Trans. Ind. Appl.*, vol. 50, no. 5, pp. 3103–3112, Sep. 2013.
- [10] K. Xu, Y. Ai and X. Wu, "Application of multi-scale feature extraction to surface defect classification of hot-rolled steels," *Int. J. Min. Met. Mater.*, vol. 20, no. 1, pp. 37–41, Jan. 2013.
- [11] X. Li, S. Tso, X. Guan, and Q. Huang, "Improving automatic detection of defects in castings by applying wavelet technique," *IEEE Trans. Ind. Electron.*, vol. 53, no. 6, pp. 1927–1934, Dec. 2006.
- [12] R. Shanmugamani, M. Sadique, and B. Ramamoorthy, "Detection and classification of surface defects of gun barrels using computer vision and machine learning," *Measurement*, vol. 60, pp. 222–230, 2015.
- [13] T. Li, J. Tsai, R. Chang, L. Ho, and C. Yang, "Pretest gap mura on TFT LCDs using the optical interference pattern sensing method and neural network classification," *IEEE Trans. Ind. Electron.*, vol. 60, no. 9, pp. 3976–3982, Sep. 2013.
- [14] L. Liu, P. Fieguth, Y. Guo, X. Wang, and M. Pietikäinen, "Local binary features for texture classification: Taxonomy and experimental study," *Pattern Recogn.*, vol. 62, pp. 135–160, 2017.
- [15] T. Ojala, M. Pietikäinen and T. Mäenpää, "Multiresolution gray-scale and rotation invariant texture classification with local binary patterns," *IEEE Trans. Pattern Anal. Mach. Intell.*, vol. 24, no. 7, pp. 971–987, Jul. 2002.
- [16] B. Abou Merhy, P. Payeur, and E. M. Petriu, "Application of Segmented 2-D Probabilistic Occupancy Maps for Robot Sensing and Navigation," *IEEE Trans. Instrum. Meas.*, vol. 57, no. 12, pp. 2827–2837, Dec. 2008.
- [17] Z. Guo, L. Zhang and D. Zhang, "A completed modeling of local binary pattern operator for texture classification," *IEEE Trans. Image Process.*, vol. 19, no. 6, pp. 1657–1663, Jun. 2010.
- [18] S. Liao, M.W. Law and A.C. Chung, "Dominant local binary patterns for texture classification," *IEEE Trans. Image Process.*, vol. 18, no. 6, pp. 1107–1118, May 2009.
- [19] T. Ahonen, A. Hadid and M. Pietikäinen, "Face recognition with local binary patterns," in *ECCV*, Berlin, Heidelberg, 2004, pp. 469–481.
- [20] Y. Yin, X. Wang, D. Xu, F. Liu, Y. Wang, and W. Wu, "Robust Visual Detection–Learning–Tracking Framework for Autonomous Aerial Refueling of UAVs," *IEEE Trans. Instrum. Meas.*, vol. 65, no. 3, pp. 510–521, 2016.
- [21] L. Liu, P. Fieguth, M. Pietikäinen, *et al.* "Median robust extended local binary pattern for texture classification," *IEEE Trans. Image Process.*, vol. 25, no. 3, pp. 1368–1381, Mar. 2016.
- [22] N. Karimi, R. Ranjbarzadeh Kondrood, and T. Alizadeh, "An intelligent system for quality measurement of Golden Bleached raisins using two comparative machine learning algorithms," *Measurement*, vol. 107, pp. 68–76, 2017.
- [23] R. Nithya, and B. Santhi, "Application of texture analysis method for mammogram density classification," *J. Instrum.*, vol. 12, Jul. 2017.
- [24] H. Z. Chen, J. X. Wang, J. Y. Li, and B. P. Tang, "A texture-based rolling bearing fault diagnosis scheme using adaptive optimal kernel time frequency representation and uniform local binary patterns," *Meas. Sci. Technol.*, vol. 28, no. 3, Mar. 2017.
- [25] S. R. Aghdam, E. Amid and M. F. Imani, "A fast method of steel surface defect detection using decision trees applied to LBP based features," in *IEEE Ind. Electron. Appl.*, 2012, pp. 1447–1452.
- [26] Q. Luo, Y. Sun, P. Li, O. Simpson, L. Tian, and Y. He, "Generalized Completed Local Binary Patterns for Time-Efficient Steel Surface Defect Classification," *IEEE Trans. Instrum. Meas.*, vol. 68, no. 3, pp. 776–779, Mar. 2019.
- [27] X. Lu, X. Li, and L. Mou, "Semi-supervised multitask learning for scene recognition," *IEEE Trans. Cybern.*, vol. 45, no. 9, pp. 1967–76, Sep. 2015.
- [28] X. Lu, X. Zheng, and Y. Yuan, "Remote sensing scene classification by unsupervised representation learning," *IEEE Trans. Geosci. Remote Sens.*, vol. 55, no. 9, pp. 5148–5157, 2017.
- [29] T. Ojala, T. Mäenpää, M. Pietikäinen, *et al.* "Outex - New framework for empirical evaluation of texture analysis algorithms," in *Proc. IEEE Int. Conf. Pattern Recogn.*, 2002, pp. 701–706.
- [30] RAMON Inc., Changsha, China, "RAMON surface quality detection system for continuous rolling [Online]," Dec., 2017, Available: <http://www.ramon.com.cn/TemplateEN/content.aspx?nodeid=169&page=ContentPage&contentid=1520>.
- [31] X. Tan and B. Triggs, "Enhanced local texture feature sets for face recognition under difficult lighting conditions," *IEEE Trans. Image Process.*, vol. 19, no. 6, pp. 1635–1650, Jun. 2010.
- [32] Y. Zhao, D.-S. Huang, and W. Jia, "Completed local binary count for rotation invariant texture classification," *IEEE Trans. Image Process.*, vol. 21, no. 10, pp. 4492–4497, Oct. 2012.
- [33] Y. Guo, G. Zhao, and M. Pietikäinen, "Discriminative features for texture description," *Pattern Recogn.*, vol. 45, no. 10, pp. 3834–3843, Oct. 2012.
- [34] A. Fathi and A. R. Naghsh-Nilchi, "Noise tolerant local binary pattern operator for efficient texture analysis," *Pattern Recognit. Lett.*, vol. 33, no. 9, pp. 1093–1100, Jul. 2012.
- [35] J. Ren, X. Jiang, and J. Yuan, "Noise-resistant local binary pattern with an embedded error-correction mechanism," *IEEE Trans. Image Process.*, vol. 22, no. 10, pp. 4049–4060, Oct. 2013.
- [36] X. Qi, Y. Qiao, C. Li, and J. J. Guo, "Multi-scale joint encoding of local binary patterns for texture and material classification," in *Proc. Brit. Mach. Vis. Conf. (BMVC)*, 2013, pp. 1–11.
- [37] X. Qi, R. Xiao, C.-G. Li, Y. Qiao, J. Guo, *et al.*, "Pairwise rotation invariant co-occurrence local binary pattern," *IEEE Trans. Pattern Anal. Mach. Intell.*, vol. 36, no. 11, pp. 2199–2213, Nov. 2014.
- [38] X. Hong, G. Zhao, M. Pietikäinen, and X. Chen, "Combining LBP difference and feature correlation for texture description," *IEEE Trans. Image Process.*, vol. 23, no. 6, pp. 2557–2568, Jun. 2014.